2026 IEEE International Conference on Robotics and Automation (ICRA 2026)
June 1-5, 2026. Vienna, Austria

In-Situ Automated Robotic Crown Preparation with MPC-Based Adaptive Control

Heng Liu[1], Huayu Fang[2], Shizhu Bai[2], Yimin Zhao[2], Junchen Wang[1,*]

Abstract— **Crown preparation aims to create an optimal foundation for durable and functional restoration by reshaping the tooth with a cutting tool. Robotic crown preparation has emerged as a promising approach to overcome the inherent limitations of manual procedures, yet challenges remain in achieving efficient cutting path generation, collision-free orientation adjustment and precise cutting path following, since the oral cavity is a confined space with the target tooth tightly surrounded by other teeth. This paper introduces a novel, in-situ automated robotic full crown preparation system comprising (1) Preoperative Path Planning: generating high-efficiency universal cutting paths based on tooth morphological features; (2) Intraoral Collision Avoidance: optimizing the cutting tool's orientation within the constrained oral cavity; (3) MPC-Based Adaptive Control: modulating the path-following feed rate using model predictive control (MPC) according to intraoperative force feedback. The proposed system was thoroughly validated on a human head phantom targeting a permanent tooth to simulate a real clinical scenario, yielding an average root-mean-square (RMS) error (tooth shape after preparation) of 0.17 mm and an overall mean execution time of 347.77 s, achieving a 74.2% improvement in cutting efficiency over state-of-the-art methods. A comparative evaluation against conventional dental guides further demonstrates its technical feasibility and significant potential for clinical translation.**

I. Introduction

When a tooth is structurally compromised by conditions such as dental caries, trauma, or pulpitis, the primary treatment objectives are the removal of diseased tissue and the restoration of the tooth's form and function. Following the elimination of pathological tissues and an assessment of the remaining sound tooth structure, preparation is essential to create the appropriate spatial and morphological foundation for the final restoration [1]. The core principles of this process are to ensure adequate restoration strength, maximize the preservation of healthy tooth structure, and establish optimal retention and resistance form.

Tooth preparation techniques range from minimally invasive veneers and inlays/onlays to more extensive full crown preparations. Full crown preparation is particularly complex, requiring significant circumferential reduction to achieve the necessary retention and material thickness. The technical challenge lies in balancing precise axial reduction and occlusal clearance with conservative tooth structure removal, all while ensuring well-defined marginal geometry (e.g., chamfer margins), continuous surface contours, and appropriate convergence angles.

The advent of CAD/CAM technologies has introduced digital workflows into this process [2]. For instance, Taha et al. demonstrated that a digitally-guided system for full-mouth rehabilitation allows for more accurate abutment preparation compared to conventional methods [3]. However, patient-specific surgical guides introduce additional design steps and, due to their static, rigid nature, lack the flexibility for intraoperative adjustments, limiting their precision in crown preparation workflows [4].

To overcome these limitations, robotic tooth preparation systems have emerged as a promising alternative [5], where a cutting tool is attached to the robotic arm for tooth reshaping. Significant research has focused on optimizing the preparation process. Sun et al. developed a trajectory optimization strategy based on five key tooth morphology parameters [6] and proposed an iso-material removal rate algorithm to suppress crack propagation [7]. Concurrently, Jiang et al. developed a thermo-mechanical coupling model to optimize grinding parameters [8] and introduced an improved algorithm for robotic joint angle optimization [9]. Despite these advances, a critical gap remains. Existing trajectory planning and optimization strategies often fail to fully incorporate tooth morphological features into the planning process. This oversight can lead to inefficient tool paths and extended preparation times. A more intelligent, feature-aware planning framework is therefore essential to bridge the gap between laboratory innovation and routine clinical use.

Notably, advanced control strategies such as model predictive control (MPC) [10] and obstacle-avoidance optimization [11] have demonstrated considerable effectiveness in surgical robotics for managing system constraints and dynamic interactions [12]. For instance, Duan et al. applied MPC in a lung puncture robot to regulate output force and maintain needle trajectory compliance [13]. Cursi et al. modeled the nonlinear dynamics of a tendon-driven surgical robot and addressed epistemic uncertainties through a hierarchical MPC framework [14]. Similarly, Koptev et al. proposed a sampling-based MPC approach to modulate joint-space dynamical systems, thereby generating collision-free and kinematically feasible motion trajectories [15]. Despite these significant advances in surgical robotics, several critical challenges persist when attempting to apply such methodolo-

This work was supported in part by the Natural Science Foundation of China under Grant 62573022, Grant U22A2051; and in part by the Natural Science Foundation of Beijing Municipality under Grant L232037. (*Corresponding author: Junchen Wang*)

[1]H. Liu and J. Wang are with the School of Mechanical Engineering and Automation, Beihang University, Beijing 100191, China. wangjunchen@buaa.edu.cn

[2]H. Fang, S. Bai, and Y. Zhao are with the State Key Laboratory of Oral & Maxillofacial Reconstruction and Regeneration, The Fourth Military Medical University, Xi'an 710032, China.

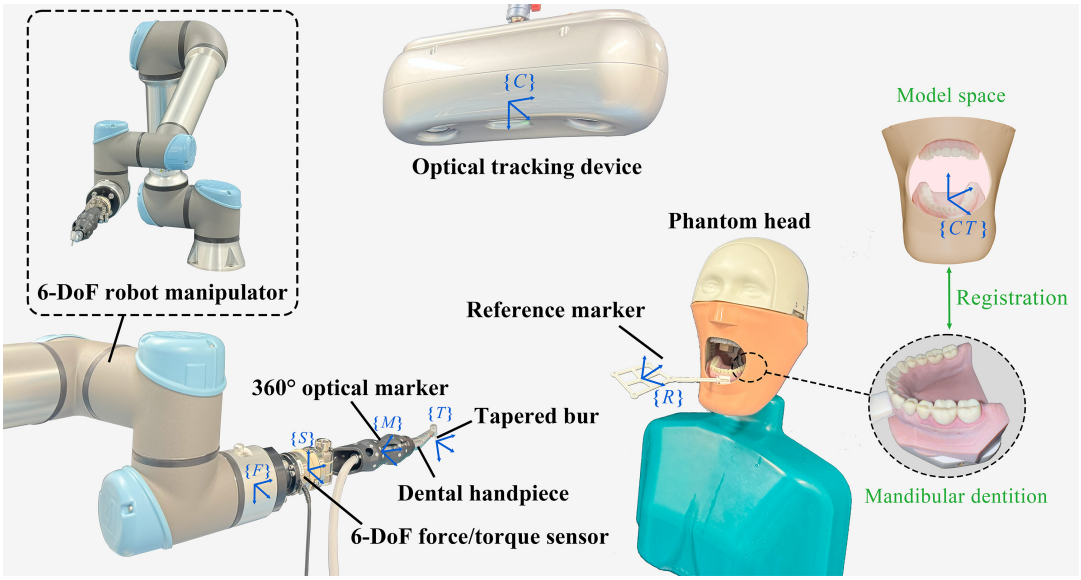

Fig. 1: Schematic of the proposed in-situ automated robotic system for full crown tooth preparation. The system consists of a 6-DoF robotic arm with a force/torque sensor, an optical tracking device, a dental handpiece with a 360° optical marker, and a tapered bur as the cutting tool.

gies to robotic tooth preparation.

1) **Inefficiency in current preoperative path planning:** Existing occlusal surface preparation schemes, which predominantly rely on layer-by-layer milling strategies, are inefficient and time-consuming. These methods often produce ridges between toolpaths, limiting their clinical applicability.
2) **Inadequate intraoral collision avoidance strategies:** Most current experimental validations are conducted on simplified models, such as embedded plaster or single-tooth setups, which fail to represent the complete dentition or the constrained and complex intraoral environment.
3) **Lack of adaptive cutting speed adjustment:** Current systems typically operate at a constant feed rate along predefined paths without incorporating real-time dynamic feedback. This results in limited adaptability to variations in material thickness and hardness.

To address these challenges, we propose an in-situ automated robotic system for full crown preparation. The system utilizes a novel path planning strategy that preoperatively generates all preparation paths based on intrinsic tooth morphology. By fully leveraging the lateral cutting edges of a tapered bur, our method significantly enhances material removal efficiency compared to conventional techniques. This strategy supports parametric design optimization to achieve the ideal preparation geometry and allows precise clinical fine-tuning prior to surgery. Furthermore, our approach incorporates proactive collision avoidance between the cutting tool and dentition by optimizing tool orientation, thereby ensuring safe and collision-free operation within the confined intraoral space. Integrating preoperative material removal data with intraoperative feedback–such as interaction forces and real-time positional errors–an adaptive MPC framework dynamically adjusts system parameters. This enables indirect estimation of material hardness and optimizes the feed rate while consistently maintaining preparation accuracy.

II. Methods

A. System Overview

Fig. 1 illustrates the proposed in-situ automated robotic system. A cutting tool (dental handpiece with a tapered bur) with a 360° optical marker are mounted to the flange of a six degrees of freedom (6-DoF) robot via a 6-DoF force/torque sensor. A phantom head serves to simulate a patient with realistic oral environment. A reference marker is attached to the mandibular for patient-image registration which calculates the mapping $\boldsymbol{T}_{CT}^{R}$ between the reference marker's frame $\{R\}$ and the preoperative model space $\{CT\}$. A hand-eye calibration procedure establishes the spatial transformation $\boldsymbol{T}_{M}^{F}$ between the robot flange frame $\{F\}$ and the 360° optical marker frame $\{M\}$. By a tool tip calibration procedure, the relationship $\boldsymbol{T}_{M}^{T}$ between the tool tip frame $\{T\}$ and frame $\{M\}$ is determined. The origin of $\{T\}$ is tip of the tapered bur and the z-axis is the rotational axis of the tapered bur. During the procedure, the optical tracking device (frame $\{C\}$) continuously acquires the poses of $\{M\}$ and $\{R\}$ to obtain $\boldsymbol{T}_{C}^{M}$ and $\boldsymbol{T}_{R}^{C}$. $\boldsymbol{T}_{F}^{B}$ is obtained by robot's forward kinematics. The final transformation $\boldsymbol{T}_{CT}^{B}$ from the robot base frame $\{B\}$ to $\{CT\}$ is given by

$$\boldsymbol{T}_{CT}^{B} = \boldsymbol{T}_{F}^{B}\,\boldsymbol{T}_{T}^{F}\,\boldsymbol{T}_{M}^{T}\,\boldsymbol{T}_{C}^{M}\,\boldsymbol{T}_{R}^{C}\,\boldsymbol{T}_{CT}^{R}. \tag{1}$$

B. Preoperative Path Planning

We propose a generalized approach for full crown preparation planning, which consists of four essential stages:

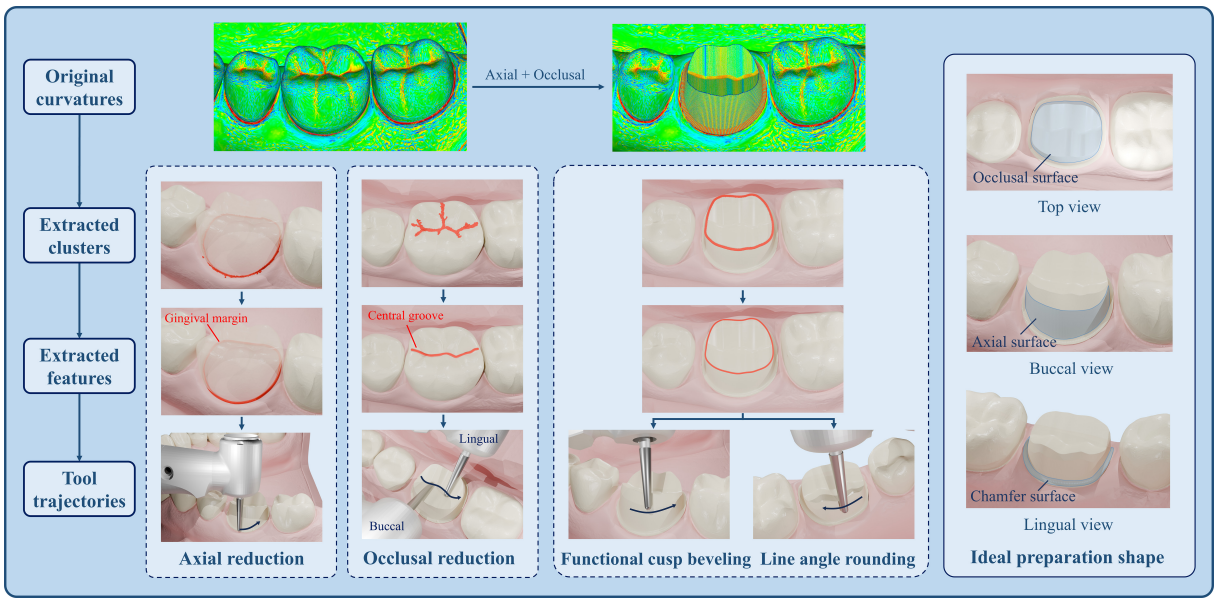

Fig. 2: Schematic of the proposed preoperative path planning process, incorporating the generation of the ideal preparation shape and three characteristic surfaces. The workflow transforms the original curvatures into four staged tool paths: axial reduction, occlusal reduction, functional cusp beveling, and line angle rounding.

axial reduction, occlusal reduction (including buccal and lingual), functional cusp beveling, and line angle rounding. In this process, three characteristic surfaces–the axial surface, occlusal surface, and chamfer surface–are generated to facilitate subsequent evaluation. The planning workflow and the aforementioned surfaces are illustrated in Fig. 2. This method utilizes morphological features of the target tooth, such as the gingival margin and central groove, as references for axial and occlusal reductions, respectively.

The specific implementation of each stage is as follows:

- **Axial Reduction:** First, a mesh model of the teeth is generated from preoperative cone beam computed tomography (CBCT) data. Point clusters corresponding to the gingival margin and the central groove are then identified from the model using curvature thresholding near the target tooth. The gingival margin, which exhibits a circular morphology, is processed using the DBSCAN algorithm [16] to remove noise and extract its main component. This component is divided into angular sectors in polar coordinates centered at the cluster center. Within each sector, the point with the smallest average radius is selected as part of the skeletal curve. A B-spline curve is fitted to these points and smoothed, followed by re-sampling at predefined intervals to generate a uniformly distributed set of points. Next, the long axis of the target tooth is estimated using the RANSAC algorithm [17]. The tapered bur is tilted from this axis toward the center of the gingival margin to achieve an appropriate convergence angle, producing a continuous and smooth chamfer finish line.
- **Occlusal Reduction:** The central groove cluster is processed similarly. A neighbor graph is constructed from the cluster, and the Dijkstra algorithm is applied to extract the shortest-path skeleton. Subsequent smoothing and resampling steps mirror those applied to the gingival margin. The buccal and lingual tool paths both reference the central groove curve. The tool orientation is determined by computing the cross product between the fitted surface normals and the fitted central groove tangent vector. This planning strategy produces a smooth, ridge-free occlusal surface with high efficiency and facilitates collision avoidance within the confined intraoral environment.
- **Functional Cusp Beveling & Line Angle Rounding:** Upon finalizing the axial and occlusal designs, a preliminary idealized preparation shape is automatically generated along with its associated curvature data. Functional cusp bevel and line angle are similarly extracted based on curvature characteristics. After obtaining the feature curves, the surface is segmented into buccal and lingual regions to identify the primary functional cusp bevel and line angle. For the functional cusp bevel, a dynamic convergence concept is introduced to determine the tapered bur's orientation. Custom deflection angles are assigned to key points along the functional cusp path. The tapered bur is tilted medially from the tooth's long axis while simultaneously moving axially, engaging its lateral cutting edges to create a smooth and rounded bevel. A comparable strategy is applied for rounding line angles. To achieve uniform chamfer dimensions while preserving natural anatomy, the tapered bur is tilted along the surface normal of the line angle curve. This orientation enables controlled use of the lateral cutting edges to produce smoothly rounded contours.

C. Intraoral Collision Avoidance

After generating the 5-DoF (tip position and axis direction) path of the tapered bur (i.e., the path of frame $\{T\}$), a sequence of tip positions and corresponding rotational axis vectors $\boldsymbol{z}_i$ in the $\{CT\}$ frame is obtained. The remaining problem is to determine the last degree of the freedom in order to determine the full pose of $\{T\}$. To address this, we propose a two-step optimization method for refining tool orientations. Specifically, while keeping the tool's z-axis fixed, the method aims to achieve the smooth and collision-free (with surrounding teeth) transition among the orientation sequence.

When the robot is at its ready state for task execution, the current rotation of $\{T\}$ with respect to $\{CT\}$ denoted by $\boldsymbol{R}_T^{CT}$ can be known through transform chain. To minimize the required rotation of the robot end-effector, we assign an initial rotation $\boldsymbol{R}_i$ for each path point as:

$$\boldsymbol{R}_i = \exp\left(\left[\frac{\boldsymbol{z}_T \times \boldsymbol{z}_i}{\|\boldsymbol{z}_T \times \boldsymbol{z}_i\|}\right]_\times \arccos(\boldsymbol{z}_T \cdot \boldsymbol{z}_i)\right) \boldsymbol{R}_T^{CT}, \quad (2)$$

where $\boldsymbol{z}_T$ is the last column vector of $\boldsymbol{R}_T^{CT}$, meaning the current axial direction of the tool expressed in $\{CT\}$. This construction ensures the minimum rotation of the robot to align the current z-axis of the $\{T\}$ frame with the planned orientation.

Next, with the initial $\boldsymbol{R}_i$, orientation optimization is performed for collision-free path. The phantom head undergoes intraoral scanning and computed tomography imaging, followed by registration of the resulting two modalities to reconstruct the complete dentition of the maxilla and mandible. These regions are designated as critical avoidance zones, as the primary principle in tooth preparation is to prevent damage to adjacent teeth and surrounding gingival tissues.

For each path point, a binary search sampling is performed in the vicinity of $\boldsymbol{R}_i$ in terms of additional rotation angle θ_i. Bounding volume hierarchies (BVHs) are constructed for the maxilla, mandible, and the dental handpiece to enable accelerated minimum distance queries [18]. The resulting boolean sequences obtained from the discrete angle samples are subsequently merged into collision-free intervals, which can be expressed as

$$\mathcal{I}_i = \{[l_{i,k}, u_{i,k}]\}_{k=1}^{m_i}, \quad (3)$$

where $\mathcal{I}_i$ denotes the set of feasible angular intervals for the i-th path point, and $[l_{i,k}, u_{i,k}]$ represents the k-th continuous sub-interval. To eliminate sampling errors introduced by the finite sampling resolution, a contraction operation is applied to each interval. The longest remaining interval is then selected as the feasible domain I_i.

$$\begin{aligned} &[l_{i,k}, u_{i,k}] \mapsto [l_{i,k} + \delta, u_{i,k} - \delta], \quad \delta > 0, \\ &I_i = \arg \max_{[l_{i,k}, u_{i,k}] \in \mathcal{I}_i} (u_{i,k} - l_{i,k}). \end{aligned} \quad (4)$$

The problem of generating a smooth angle sequence within feasible domain can be naturally formulated as a constrained quadratic optimization problem. Let $\boldsymbol{\theta} = [\theta_0, \theta_1, \ldots, \theta_{n-1}]^\top$ denote the angle sequence, and $c_i = (l_i + u_i)/2$ be the midpoint of the feasible domain $I_i = [l_i, u_i]$ for each point i. The objective is to compute the optimal angles $\boldsymbol{\theta}^*$ that stay close to the interval midpoints (to avoid collisions) while ensuring smooth transitions between consecutive angles. This leads to the following quadratic programming (QP) problem:

$$\begin{aligned} \boldsymbol{\theta}^* = \arg\min_{\boldsymbol{\theta}} &\sum_{i=0}^{n-1} w_c(\theta_i - c_i)^2 + \sum_{i=0}^{n-2} w_s(\theta_{i+1} - \theta_i)^2 \\ &\text{s.t. } l_i \le \theta_i \le u_i, \quad i = 0, 1, \ldots, n-1, \end{aligned} \quad (5)$$

where w_c and w_s are weighting factors controlling the trade-off between midpoint adherence and smoothness. The optimal sequence $\boldsymbol{\theta}^*$ can be obtained and applied to the original poses $(\boldsymbol{p}_i, \boldsymbol{R}_i)$ to produce the adjusted trajectory:

$$\mathcal{T}' = \{(\boldsymbol{p}_i, \boldsymbol{R}_i\, \boldsymbol{R}_z(\theta_i^*))\}_{i=1}^n. \quad (6)$$

where $\boldsymbol{R}_z(\theta_i^*)$ denotes the rotation corresponding to the smoothed angle θ_i^*. This principle is schematically illustrated in Fig. 3.

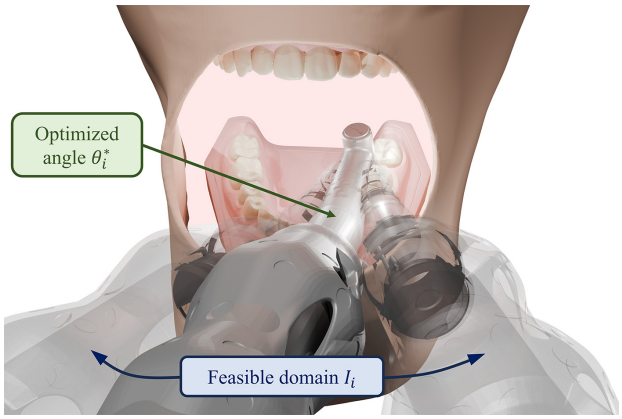

Fig. 3: Feasible domain I_i obtained from collision detection and the selected optimized angle θ_i^*.

The same approach can also be applied to seamlessly connect consecutive path segments. Discrete path points within each segment are interpolated separately in position and orientation space, using cubic splines to generate C^2-continuous positional trajectories [19] and spherical linear interpolation of quaternions for smooth rotational transitions [20].

The proposed optimization generates a path that preserves the original positions and adjusts orientations near the midpoints of the feasible domain, promoting smooth motion and avoiding collisions.

D. MPC-Based Adaptive Control

During robotic tooth preparation, the robot must accurately follow preoperatively planned paths at an appropriate feed rate while maintaining cutting precision and operational safety. Inspired by clinical practice, in which dentists dynamically adjust the feed rate based on factors such as cutting

force and material removal, we developed an adaptive MPC strategy for real-time feed rate regulation. This controller dynamically optimizes system parameters in response to intraoperative interaction forces and real-time tracking errors [21], allowing indirect estimation of material hardness to maximize cutting efficiency while consistently satisfying accuracy requirements [22].

The model utilizes the arc-length progress variable s along the tool path as the state variable and the current feed rate factor α as the control input. Defining $v_{\max}$ as the maximum allowable feed rate, L as the total path length, and T_s as the sampling period. During preoperative planning, the dynamic material removal volume along the tool path can be precomputed based on the planned path. Through numerical differentiation, the volumetric removal rate per unit arc length is obtained and denoted as $Q(s_k)$. The actual material removed at time step k can then be calculated as:

$$\Delta V_k = Q(s_k) \cdot v_{\max} \alpha_k T_s. \tag{7}$$

The removal volume is normalized to yield the normalized removal intensity $\widetilde{Q}(s_k) = Q(s_k)/Q_{\max}$, where $Q_{\max}$ denotes the maximum removal volume within the current path segment. To achieve high feed rates while simultaneously preventing tool overload, we propose the following MPC design:

$$\min_{\{\alpha_k\}_{k=0}^{N-1}} \sum_{k=0}^{N-1} \left[w_1 (\widetilde{Q}(s_k)\alpha_k)^2 + w_2 (1-\alpha_k)^2 \right]$$

$$\text{s.t.} \begin{cases} s_{k+1} = s_k + \dfrac{v_{\max} T_s}{L}\,\alpha_k, & k = 0, \dots, N-1, \\ s_0 = 0, & \\ 0 \le s_k \le 1, & k = 0, \dots, N, \\ 0 \le \alpha_k \le 1, & k = 0, \dots, N-1. \end{cases} \tag{8}$$

where N denotes the prediction horizon, while w_1 and w_2 are weighting coefficients penalizing excessive removal intensity and low feed rates, respectively. An appropriate choice of the weight ratio w_1/w_2 balances the trade-off between constraining the cutting load and maximizing the feed rate.

Building upon the aforementioned model, the MPC controller performs receding horizon optimization at each control cycle. This strategy optimizes a finite sequence of control inputs α_k over a limited prediction horizon and recomputes the sequence upon advancing to the next cycle. Leveraging the efficient Quadratic Programming solver OSQP [23], the controller ensures optimization computations are completed within sub-millisecond timeframes.

Accounting for the anisotropic mechanical properties of dental tissues and the variability across individuals, the ratio of weighting coefficients w_1/w_2 requires dynamic adjustment at each time step. Inspired by the concept of gain scheduling, the magnitudes of force and position errors are mapped to a risk index [24], which serves as the basis for adaptive adjustment of the control weights [25].

During the procedure, the filtered actual position of the tool tip $\boldsymbol{p}_{\text{act}}$ is computed using forward kinematics, while the reference position $\boldsymbol{p}_{\text{ref}}$ on the planned path is simultaneously obtained. In addition, the filtered real-time interaction force $\boldsymbol{F}_k$ between the tool and the dental tissues is measured through the end-effector force sensor. The Euclidean norms of these quantities are then computed and normalized as follows:

$$\begin{cases} F_{\text{norm},\,k} = \min\left(\dfrac{\|\boldsymbol{F}_k\|_2}{F_{\lim}}, 1\right), \\ e_k = \min\left(\dfrac{\|\boldsymbol{p}_{\text{act}} - \boldsymbol{p}_{\text{ref}}\|_2}{e_{\lim}}, 1\right), \end{cases} \tag{9}$$

where $F_{\lim}$ and $e_{\lim}$ are the maximum allowable interaction force and position error, respectively.

The normalized force and position error are linearly combined to obtain a unfiltered risk index:

$$z_k = \lambda_f F_{\text{norm},\,k} + \lambda_p e_k, \tag{10}$$

where λ_f and λ_p are weighting coefficients reflecting the relative contributions of the force and position error to the overall risk index.

To obtain a smoothed estimate of the risk index, the unfiltered risk index z_k is filtered using a scalar Kalman filter. The filtered value σ_k leverages past observations to reduce noise and is confined to the range $[0, 1]$. The dynamic weighting ratio $\rho_k = w_1/w_2$ is generated through linear interpolation:

$$\rho_k = \rho_{\min} + (\rho_{\max} - \rho_{\min})\,\sigma_k, \tag{11}$$

where $\rho_{\min}$ and $\rho_{\max}$ denote the minimum and maximum values of the weighting ratio, respectively. This dynamic weighting ratio is incorporated into the MPC cost function to adaptively balance cutting efficiency and precision, thereby achieving an optimal trade-off while ensuring surgical safety.

III. Experiments and Results

A. Experimental Setup

The objective of our experiments is to evaluate the accuracy and efficiency of the proposed in-situ automated robotic system. All experiments were performed on tooth 36 (according to the FDI tooth-numbering system). The experimental study comprises three main stages. First, intraoral collision avoidance strategies are evaluated through simulation. Subsequently, the robotic system executes the full tooth preparation procedure on a phantom head model. Finally, a graduate student in prosthodontics performs the preparation using digital surgical guides. The outcomes are quantitatively compared with those obtained from the robotic experiment.

The experimental setup included the following components: an optical tracking system (FusionTrack 250, Atracsys, Switzerland), a force/torque sensor (ATI Mini, Apex, USA), a 6-degree-of-freedom robotic arm (UR5e, Universal Robots, Denmark), and a dental high-speed handpiece (CA 1:5, Bien-Air Dental, Switzerland) fitted with a tapered bur TR13. The robotic simulation environment and control algorithms were implemented using our laboratorys C++ software platform, which was developed within the ROS2 framework (available

at https://github.com/JunchenWang/ros2_robot_control).

B. Intraoral Collision Avoidance Experiment

In order to evaluate the intraoral collision avoidance performance, simulation experiments were conducted for the four types of preparation described above. Among these procedures, the axial surface contains the highest density of path points while the functional cusp bevel involves a relatively large change in handpiece orientation. Consequently, these two procedures were selected for demonstration.

The axial reduction and functional cusp bevel paths were discretized into 200 and 100 points, respectively. For both paths, the search interval was empirically set to $\pm 45^\circ$ with a step size of 0.5°, and the parameters w_c and w_s were set to 1 and 5. The corresponding optimal $\boldsymbol{\theta}^*$ is presented in Fig. 4.

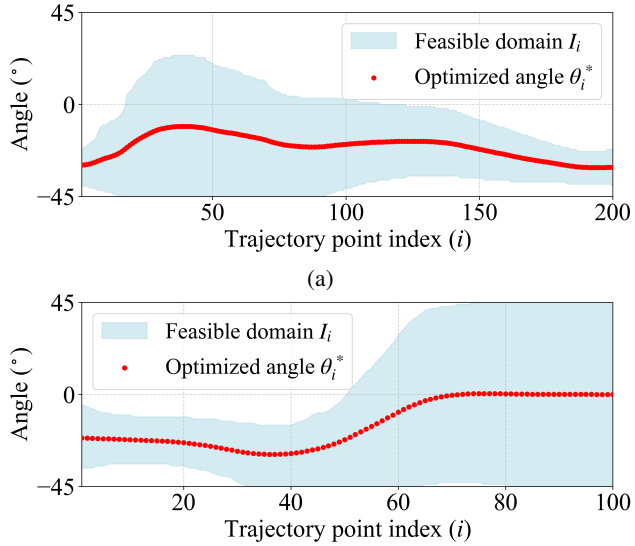

Fig. 4: Feasible domains I_i and optimized θ_i^* values. (a) Axial reduction. (b) Functional cusp beveling.

The results indicate that the proposed collision-avoidance optimization method ensures that the angles remain within the feasible domain while adjusting orientations to lie near the midpoints of the feasible ranges, thereby promoting smooth motion and minimizing the risk of singular configurations.

C. Robotic Experiment

We designed and fabricated replaceable teeth models that can be fixed inside a phantom head, as illustrated in Fig. 5(a). Before tooth preparation, the cutting tool on the end of the robotic arm was freely dragged into the mouth by the operator using an admittance controller. Subsequently, guided by an optical tracking system, the robotic system autonomously performed the complete tooth preparation procedure at a maximum feed rate of $v_{\max}$ of 0.5 mm/s, with a control cycle of 2 ms. The prediction horizon N was empirically set to 10, and the limits $F_{\lim}$ and $e_{\lim}$ were set to 4 N and 0.3 mm. The weights λ_f, λ_p and the ratio bounds $\rho_{\min}$, $\rho_{\max}$ were set to 0.6, 0.4, 1, and 3, respectively. To highlight the effectiveness of the MPC controller, constant speed path following (feed rate of 0.5 mm/s) without the MPC controller was also performed. For comparison between robotic tooth preparation and conventional tooth preparation, we also conducted tooth preparation experiments based on cutting guides. In total, 15 trials were performed which were equally divided into three groups: robot with MPC, robot without MPC and 3D-printed guide. After each trial, the resulting tooth was scanned to acquire the 3D shape which was further compared with the preoperatively planned shape. The evaluation metrics included overall root-mean-square (RMS) error and region-specific RMS errors. The results are shown in Fig. 7. The actual robotic tooth preparation result from one trial are shown in Fig. 5(b) and (c). The RMS visualization and comparison results from two trials are shown in Fig. 6. In all trials, no damage was observed in the adjacent teeth or gingiva.

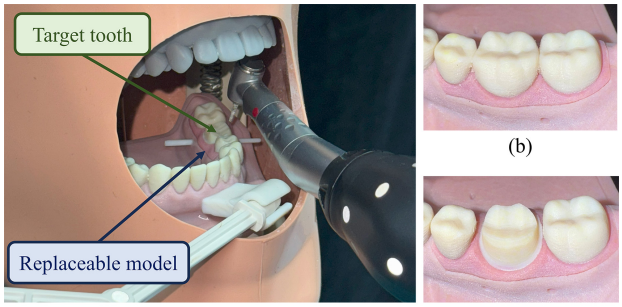

Fig. 5: Robotic experimental setup and results. (a) Replaceable model fixed in the phantom head. (b) Before preparation. (c) After preparation.

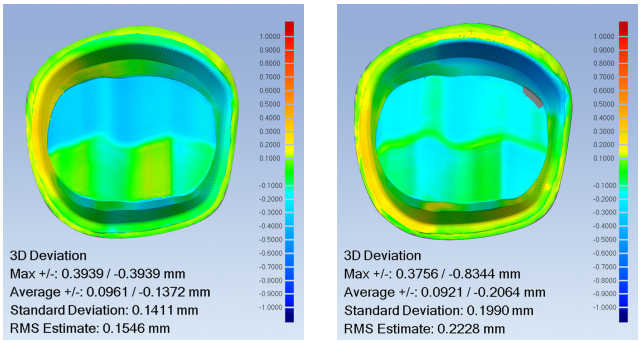

Fig. 6: Comparison of representative registration results from two trials. (a) With MPC. (b) Without MPC.

Metric results indicate that preparations using MPC exhibit a marginally lower overall RMS error (0.15 mm vs. 0.22 mm) compared to those without MPC. This improvement was particularly pronounced during axial reduction, primarily due to deeper material removal at the buccal side where maximum cutting thickness exceeded 1 mm. This interpretation

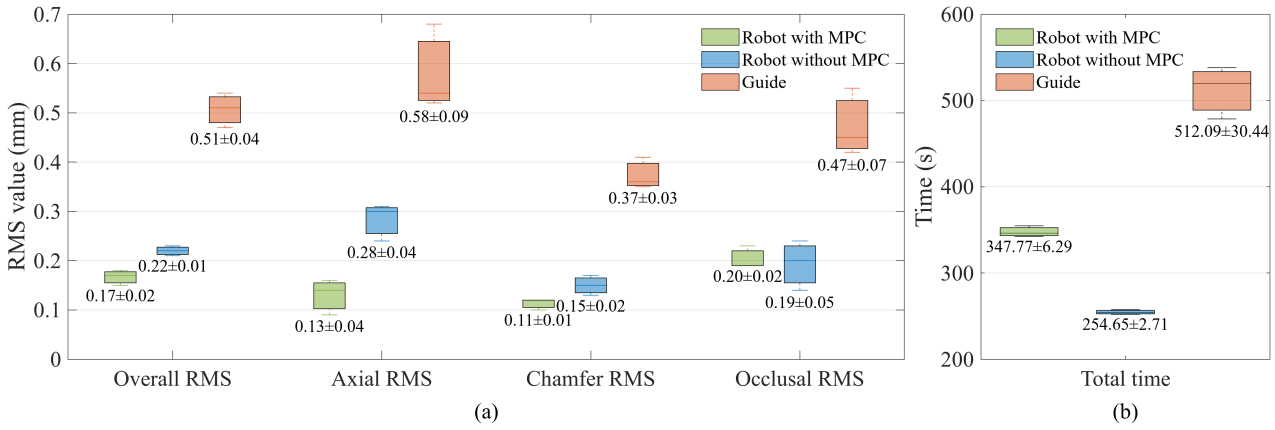

Fig. 7: Comparison of preparation accuracy on each surface (a) and total time (b) among three groups (Robot with MPC, Robot without MPC, Guide; 5 experiments each).

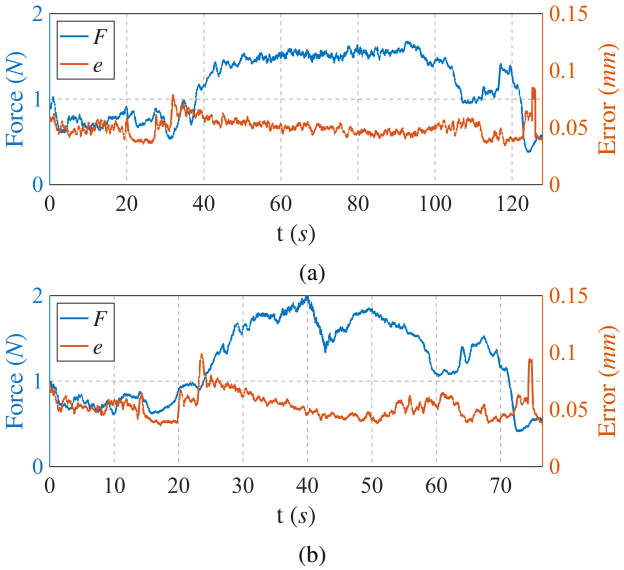

Fig. 8: The variations in interaction force F and position error e during the axial reduction step from representative trials. (a) With MPC. (b) Without MPC.

is further confirmed in Fig. 8, which shows the interaction force and the trajectory error during the axial reduction step from one trial. With MPC control, relatively stable cutting forces were maintained even in the buccal region with a greater cutting depth (50–90 s), while the positional error consistently remained below 0.08 mm. These results demonstrate the validity and efficacy of the proposed MPC-based adaptive control strategy.

D. Guide Experiment

Within full-crown preparation methodologies, preparation guides constitute one of the most accurate traditional approaches. Following the same preparation concept as the robotic preparation, a digital step-by-step guide design was performed to guide the cutting for the ideal preparation shape. As shown in Fig. 9(a)–(c), occlusal, buccolingual, and proximal guide components were sequentially fabricated.

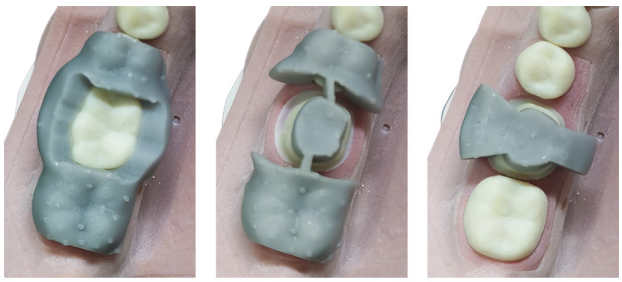

Fig. 9: Schematic illustration of the designed guides. (a) Occlusal guide. (b) Buccolingual guide. (c) Proximal guide.

Five full-crown preparations were performed using the designed preparation guides. All procedures were conducted by a prosthodontics professional following standard guided preparation protocols. After preparation, the RMS errors and total preparation time were computed, and both their mean and standard deviation were calculated. These results are reported in Fig, 7. Quantitative analysis revealed that the guided group exhibited significantly higher RMS errors compared to the robotic groups, with longer preparation time as well.

IV. Discussion

The proposed robotic system combines a novel path planning strategy with MPC-based adaptive control to minimize preparation time while maintaining accuracy. Compared to state-of-the-art layer-by-layer methods [6], [9], the proposed system achieves comparable precision while substantially reducing preparation time from 1350 s to 347.77 s, achieving a 74.2% efficiency improvement. However, defects in the gingival margin or central groove features of a patient's target tooth may compromise the accuracy of feature extraction. Future research could explore the integration of advanced techniques to predict and extract these critical morphological features.

The higher RMS error without MPC was mainly due to uneven grinding thickness during axial reduction, where larger average removal depths induced greater interaction forces–particularly on the buccal side, leading to positional deviations and slightly larger chamfer errors. In contrast, the occlusal surface showed low sensitivity to MPC because of its shallow cutting depth. Overall, the system achieved an accuracy level that meets clinical requirements.

In terms of collision avoidance, the current solution only considers the surrounding dentition for collision avoidance. However, for clinical application, it is necessary to account for dynamic variations within a patient's oral cavity, such as the movement of the tongue or other dental tools. Future work could incorporate depth cameras or advanced sensing techniques to capture these changes in real time and enhance the capability of collision avoidance.

Experimental results showed slightly higher RMS errors on the occlusal surface than on the axial and chamfer surfaces, mainly due to lower 360° marker recognition accuracy at buccal and lingual postures during occlusal preparation. Future work could develop additional optimization strategies for occlusal reduction based on the existing MPC design, aiming to predict and compensate for potential errors and further enhance the system's precision.

V. Conclusion

This study presents an in-situ automated robotic full crown preparation system with MPC-based adaptive control. Experimental evaluation on the phantom head yielded an average RMS of 0.17 mm and an average preparation time of 347.77 s, representing a 74.2% improvement in efficiency compared to state-of-the-art methods. Future work will focus on refining the proposed system and conducting comprehensive validation studies to rigorously evaluate its clinical applicability.

References

[1] C. Winkelmeyer, S. Wolfart, and J. Marotti, "Analysis of tooth preparations for zirconia-based crowns and fixed dental prostheses using stereolithography data sets," *Journal of Prosthetic Dentistry*, vol. 116, no. 5, pp. 783–789, Nov. 2016.

[2] N. Dai, Y. Zhong, H. Liu, F. Yuan, and Y. Sun, "Digital modeling technology for full dental crown tooth preparation," *Computers in Biology and Medicine*, vol. 71, pp. 190–197, Apr. 2016.

[3] Y. Taha, F. Raslan, A. Ali, and M. Roig, "Guided tooth preparation device fabricated with a complete digital workflow: A dental technique," *The Journal of Prosthetic Dentistry*, vol. 125, no. 2, pp. 221.e1–221.e4, Feb. 2021.

[4] M. Robles, C. A. Jurado, F. Floriani, S. Rojas-Rueda, P. Garcia, and F. X. Azpiazu-Flores, "3D-printed tooth reduction guide for minimally invasive veneer preparations a case report," *International Journal of Esthetic Dentistry*, vol. 19, no. 4, pp. 348–359, WIN 2024.

[5] D. Wu, J. Jiang, J. Pan, K. Qian, and Z. Xue, "Root canal preparation robot based on guiding strategy for safe remote therapy: System design and feasibility study (2023)," *IEEE/ASME Transactions on Mechatronics*, vol. 30, no. 1, pp. 84–95, Feb. 2025.

[6] J. Sun, J. Jiang, C. Wang, Z. Xue, A. Li, and J. Pan, "Trajectory optimization for tooth preparation robot based on P-MRSD algorithm," *IEEE Transactions on Automation Science and Engineering*, pp. 1–1, 2025.

[7] J. Sun, J. Jiang, Z. Xue, J. Pan, and D. Qiao, "Layered preparation method for cracked tooth preparation robot based on iso-MRR algorithm," *IEEE/ASME Transactions on Mechatronics*, pp. 1–12, 2024.

[8] J. Jiang, B. Ma, J. Sun, Y. Zhang, J. Pan, and S. Zhou, "Crack extension analysis and parameter optimization in robot-assisted cracked tooth preparation process: Finite element analysis and experiment," *International Journal for Numerical Methods in Biomedical Engineering*, vol. 41, no. 7, p. e70070, Jul. 2025.

[9] J. Jiang, Z. Xue, J. Sun, C. Wang, J. Wang, J. Pan, and T. Shen, "An OBS-WA algorithm for pose optimization of a tooth preparation robot end-effector in confined spaces," *IEEE Journal of Biomedical and Health Informatics*, pp. 1–14, 2025.

[10] Y. Song, L. Zhu, J. Li, J. Deng, C. Wang, and A. Song, "MPC design of a continuum robot for pulmonary interventional surgery using koopman operators," *IEEE Robotics and Automation Letters*, vol. 9, no. 12, pp. 10 819–10 826, Dec. 2024.

[11] X. Xiao, X. Li, H. Mo, Y. Shi, J. Fang, L. Li, B. Ouyang, and S. Yang, "A Shared Control Method of Multiobjective Motion Fusion for Surgical Robot," *Advanced Intelligent Systems*, vol. 7, no. 7, p. 2400806, Jul. 2025.

[12] M. Khadem, J. O'Neill, Z. Mitros, L. da Cruz, and C. Bergeles, "Autonomous steering of concentric tube robots via nonlinear model predictive control," *IEEE Transactions on Robotics*, vol. 36, no. 5, pp. 1595–1602, Oct. 2020.

[13] X. Duan, R. He, Q. Zhao, X. Chen, and C. Li, "Unified admittance control for accurate puncture and respiration following based on disturbance observation and model predictive control," *IEEE Robotics and Automation Letters*, vol. 10, no. 4, pp. 3526–3533, Apr. 2025.

[14] F. Cursi, V. Modugno, L. Lanari, G. Oriolo, and P. Kormushev, "Bayesian neural network modeling and hierarchical MPC for a tendon-driven surgical robot with uncertainty minimization," *IEEE Robotics and Automation Letters*, vol. 6, no. 2, pp. 2642–2649, Apr. 2021.

[15] M. Koptev, N. Figueroa, and A. Billard, "Reactive collision-free motion generation in joint space via dynamical systems and sampling-based MPC," *International Journal of Robotics Research*, vol. 43, no. 13, pp. 2049–2069, Nov. 2024.

[16] M. Ester, H.-P. Kriegel, J. Sander, and X. Xu, "A density-based algorithm for discovering clusters in large spatial databases with noise," in *Proceedings of the Second International Conference on Knowledge Discovery and Data Mining*, ser. KDD'96, 1996, p. 226231.

[17] M. A. Fischler and R. C. Bolles, "Random sample consensus: a paradigm for model fitting with applications to image analysis and automated cartography," *Commun. ACM*, vol. 24, no. 6, p. 381395, Jun. 1981. [Online]. Available: https://doi.org/10.1145/358669.358692

[18] U. Schwesinger, R. Siegwart, and P. Furgale, "Fast collision detection through bounding volume hierarchies in workspace-time space for sampling-based motion planners," in *2015 IEEE International Conference on Robotics and Automation (ICRA)*, 2015, pp. 63–68.

[19] A. Müller, T. Marauli, and H. Gattringer, "Smooth invariant interpolation on lie groups with prescribed terminal conditions for robot motion planning and modeling of soft robots," in *2024 IEEE/RSJ International Conference on Intelligent Robots and Systems (IROS)*, Oct. 2024, pp. 8442–8448.

[20] G. Liu, Q. Li, B. Yang, H. Zhang, and L. Fang, "An efficient linear programming-based time-optimal feedrate planning considering kinematic and dynamics constraints of robots," *IEEE Robotics and Automation Letters*, vol. 9, no. 3, pp. 2742–2749, Mar. 2024.

[21] D. Rakovitis and D. Mronga, "Gaussian mixture likelihood-based adaptive MPC for interactive mobile manipulators," in *2024 IEEE International Conference on Robotics and Automation (ICRA)*, May 2024, pp. 1392–1398.

[22] J. Norby, A. Tajbakhsh, Y. Yang, and A. M. Johnson, "Adaptive complexity model predictive control," *IEEE Transactions on Robotics*, vol. 40, pp. 4615–4634, 2024.

[23] B. Stellato, G. Banjac, P. Goulart, A. Bemporad, and S. Boyd, "OSQP: an operator splitting solver for quadratic programs," *Mathematical Programming Computation*, vol. 12, no. 4, pp. 637–672, 2020. [Online]. Available: https://doi.org/10.1007/s12532-020-00179-2

[24] B. Hammoud, M. Khadiv, and L. Righetti, "Impedance optimization for uncertain contact interactions through risk sensitive optimal control," *IEEE Robotics and Automation Letters*, vol. 6, no. 3, pp. 4766–4773, Jul. 2021.

[25] W. Zou, P. Duan, Y. Chen, N. Yu, and L. Shi, "Variable stiffness control with strict frequency domain constraints for physical human-robot interaction," in *2020 IEEE/RSJ International Conference on Intelligent Robots and Systems (IROS)*, Oct. 2020, pp. 7146–7151.